International Conference on Space Optics—ICSO 1997

Toulouse, France

2–4 December 1997

Edited by George Otrio

Reducing the optical and x-ray stray light In the ESA XMM telescopes

Daniel de Chambure, Kees van Katwijk, Robert Laine, Jan van Casteren, et al.

International Conference on Space Optics — ICSO 1997, edited by Georges Otrio, Proc. of SPIE Vol. 10570, 105700V · © 1997 ESA and CNES · CCC code: 0277-786X/18/$18 · doi: 10.1117/12.2326469

REDUCING THE OPTICAL AND X-RAY STRAY LIGHT IN THE ESA XMM TELESCOPES

Daniel de Chambure [1], Kees van Katwijk [1], Robert Lainé [1], Jan van Casteren [1], Gary Peterson [2], Marie Côté [2], Bernd Aschenbach [3], Richard Willingale [4], Dittmar Schink[5], Albrecht Frey[5], Wolfgang Rühe[5], Yolanda Gutierrez[6], Falk Draheim[7]

(1) European Space Agency, European Space Research and Technology Centre, XMM Project, PO Box 299, 2200 AG Noordwijk, ZH The Netherlands; (2) Breault Research Organization, Tucson, United States of America; (3) Max-Planck-Institut für Extraterrische Physik, Garching, Germany; (4) University of Leicester, United Kingdom; (5) Dornier, Friedrichshafen, Germany; (6) Sener, Las Arenas, Spain; (7) Oerlikon Contraves, Zurich, Switzerland

ABSTRACT- *The high throughput X-ray spectroscopy mission XMM is the second "Cornerstone" Project in the ESA long term Programme for Space Science. This observatory has at its heart three heavily nested Wolter 1 grazing incidence X-ray telescopes which will provide a large collecting area (each 1475 cm² at 1.5 keV and 580 cm² at 8 keV). This optical system has a spatial resolution of 15-16 arcsec and, when coupled with reflection grating spectrometers and X-ray CCD cameras, it will provide a major advance in astrophysics by the end of the century.*

In this paper, we first present the design of the telescope and then describe our approach for reducing the optical and the X-ray stray light level in the telescopes. We then concentrate on the analysis performed for determining the optical and X-ray stray light levels as a function of the operational constraints. Finally, the results achieved in terms of hardware (optical and X-ray baffle) and in terms of stray light verification of the XMM telescopes are also presented.

Key Words: *ESA, XMM spacecraft, X-ray optics, optical stray light, X-ray stray light, advanced manufacturing*

1- INTRODUCTION

The X-ray Multi Mirror (XMM) spaceborn observatory, due for launch in August 1999 by an Ariane 5 launcher, has been designed as a high throughput X-ray spectroscopy mission over a broad band of energies, ranging from 0.1 to 12 keV (as presented in references[1,2]). The design of the spacecraft is dominated by a 8 meter long tube which accommodates, on one side the Mirror Support Platform with the three telescopes (see figure 1) surrounded by the Service Module and the Telescope Sun Shield and on the other side the detectors placed at the foci of each of the telescopes.

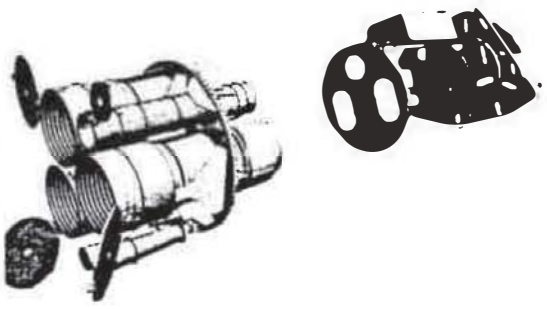

Figure 1: Inner view on the XMM spacecraft with the 3 telescopes and the 2 anticross talk stops

The optics of the three telescopes (hereafter

referred to as Mirror Modules) are each made of 58 nested Wolter1 grazing incidence mirrors, chosen to maximise the effective collecting area and they are detailed in section 2.

The detectors consist of:

three imaging X-ray CCD (Charged Coupled Device) cameras, mounted at the prime focus of each of the telescopes (EPIC instrument)

two spectrometers consisting of a strip of CCD cameras, located at the secondary focus of each of the two telescopes which are equipped with grating stacks (RGS instrument).

Since the X-ray CCD detectors are also sensitive to visible and near infrared light, it is required to limit the light level in the field of view of all the detectors in the wavelength range between 350 nm and 1000 nm, due to stray light sources outside the field of view:

$< 2.0\ 10^{5}$ photons/cm^{2}/sec for sources between an angle of 0.25° and 2.5° from the optical axis

$< 5.0\ 10^{3}$ photons/cm^{2}/sec for sources at angles larger than 2.5° from the optical axis.

The sources of the optical stray light impinging the detectors can be distinguished into two categories:

stray light going through the telescope aperture at angles larger than the field of view of the experiments (i.e. 0.25°)

leak light going through the Telescope Tube (i.e. through flanges, outgassing baffle, door interfaces, feedthrough, etc..).

Concerning optical stray light passing through the XMM telescopes, the solution adopted encompasses: a cylindrical shield and various filters for the detectors, optical baffles (see section 5) in front of the telescope apertures and two anti-cross talk stops located between the telescopes and the detectors, inside the Telescope Tube. Also, the (deployable) Telescope Sun Shield with its oblique angle towards the sun, ensures not only that direct sun light cannot enter the telescopes, but also prevents that any surface, visible from the (optical) entrance baffle apertures, can be illuminated by direct sun light for any spacecraft attitude up to 20° (pitch and roll).
Special care has been taken in the design of the structure and the interfaces of the Telescope Tube in terms of light tightness. For example, a 20 µm pinhole in the Telescope Tube on the sun side would be sufficient to flood the detectors with stray light. Its inner surface is covered with an anti reflective laminated face sheet, consisting of a 20 µm metallic foil cladded with black Kapton. Light tight seals are used in all joints between the Telescope Tube and the focal plane platform, the Mirror Support Platform, the telescopes, the feedthrough etc... Light tightness tests performed on the tube confirm the prediction that the sum of all light leaks for any allowed constellation of Earth or Sun will not exceed 10% of the above specified value for stray light sources at angles larger than 2.5°. Therefore, this paper will only address the problem of optical stray light through the telescopes (see section 3).

The XMM mirrors image the X-ray sky that comprises point sources such as stars, extended structures like supernova remnants or clusters of galaxies, and other diffuse but structured components, such as faint unresolved point sources or a truly diffuse cosmic X-ray background.
However, scattering, specular reflection, and rogue reflections from surfaces in the optics, will produce additional diffuse X-ray flux and imaging artefacts in the detectors. In other words, the image of 30 arcmin square area of the sky (EPIC field of view) can be contaminated by diffuse X-ray light background, produced by X-ray sources located outside the field of view. This background increases the detection noise, reduces the contrast of the image and modifies its spectrum in a way which is dependant on the pointing direction. This hardly affects the EPIC observations of isolated sources and RGS spectra. On the contrary, for extended objects, there is a severe limitation on the observations. These additional X-ray components must be suppressed to a maximum extent and the residuals quantified and calibrated in order to achieve the limiting sensitivity of XMM for both point sources and diffuse structures in the X-ray sky (see sections 4 and 6).

Electrons will also enter the aperture of the telescope and most probably will be scattered at shallow angles by the different elements of the telescope in the direction of the detectors. Or even worse, they might be focused by the mirrors on the CCDs, thereby increasing the background level of the detectors. They are seen by the detectors as stray light. Based on ROSAT experience, an "electron deflector" with permanent magnets has been placed in the X-ray beam, producing a high magnetic field perpendicular to the telescope axis. The prediction indicates that this tangential (more exactly toroidal) field is able to deflect sideways the most energetic electrons and even to reflect off the softer ones, thereby reducing the background at the detector to an undetectable level
Further details can be found in reference [7]

2- TELESCOPE DESIGN DESCRIPTION

The three telescopes consist of the following elements (see figure 2):

Mirror Assembly Door, which closes and protects the X-ray optics and the telescope interior against contamination during integration, test, transport, launch and early orbit phase
Entrance Baffle (detailed in section 5), which provides the stray light suppression capability in the visible wavelength range
X-ray Baffle (detailed in section 6), which blocks X-rays from outside the nominal field of view, which would otherwise reflect once on the hyperboloid section of the mirrors and would therefore cause stray light
Mirror Module (MM), the X-ray optics of the telescope, detailed hereafter
"Electron Deflector" (producing a toroidal magnetic field), right behind the mirrors (in the shadow of the spider of the MM) for diverting "soft" electrons (with energy up to 100 keV)
Reflection Grating Assembly (RGA), with a mass of 60 kg, on the backside of two out of three Mirror Modules, corresponding to the telescopes 1 and 2. It deflects roughly half of the X-ray light to a strip of CCD detectors (RGS), offset from the focal plane. It includes 182 reflection grating plates (100 x 200 mm), mounted and aligned in an Beryllium alloy structure. Each grating is replicated from a master, onto a SiC substrate.
Exit Baffle, providing a thermal environment for the gratings and the Mirror Module.

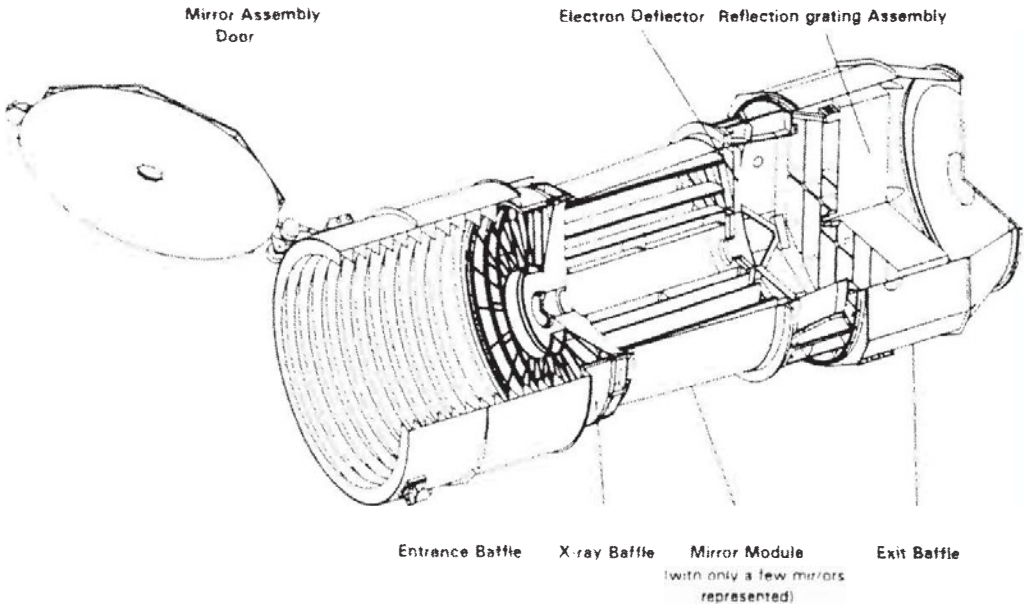

Figure 2: XMM telescope design

The XMM Mirror Module is a grazing incidence telescope (Wolter I type) which is designed to operate in the X-ray energy range of 0.1-12 keV with a focal length of 7.5 meters and with a resolution of 16 arcsec. The grazing incidence angles of the X-rays range from 17 arcmin for the smallest mirror to 40 arcmin for the largest. A Mirror Module consists of 58 nested mirror shells bonded at one end on a spider (or spoke wheel) and their supporting structure.
The optical concept of the XMM Mirror Module is shown in figure 3.

Focal length 7500 mm
Resolution
Half Energy Width
16 arcsec (0.1-12 keV)
Full Width Half Max
8 arcsec (0.1-12 keV)
Effective area
1475 cm^2 at 1.5 keV
580 cm^2 at 8 keV
Mirror diameter
Outermost 700 mm
Innermost 306 mm
Mirror length 600 mm
Packing distance 1- 5 mm
Number of mirrors 58
Mirror Module mass 425 kg

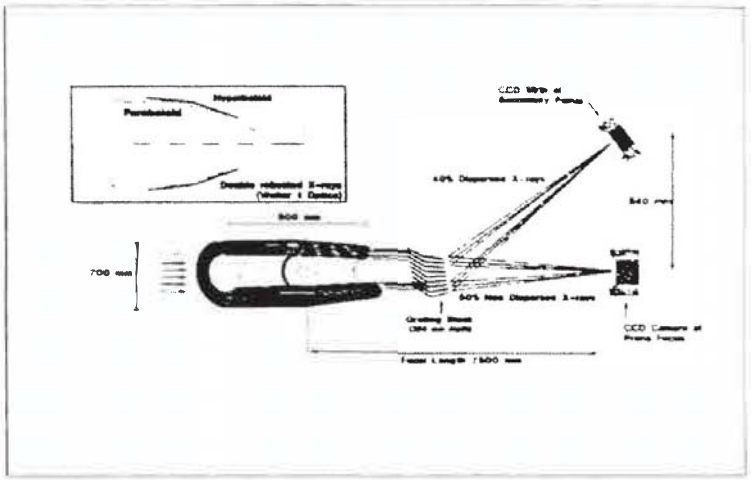

***Figure 3**: Optical design of the XMM Mirror Module with the grating assembly (RGA)*

Each mirror is a thin monolithic nickel shell which is shaped to a paraboloid surface at the front and an hyperboloid surface at the rear, for double reflection of the grazing X-rays. The 58 mirror shells, with diameters between 306 mm and 700 mm and a length of 600 mm, are mounted in a confocal and coaxial configuration. The reflective coating of the mirrors is a 250 nm layer of high purity gold. The thickness of the mirror shells ranges from 0.47 mm up to 1.07 mm, proportional to their diameter. The mirror manufacturing is based on a replication process which transfers a gold layer deposited on an highly polished master mandrel onto an electrolytic shell, which is electroformed on top of the gold layer. Details of the development of the process are given in references [5,6,7].

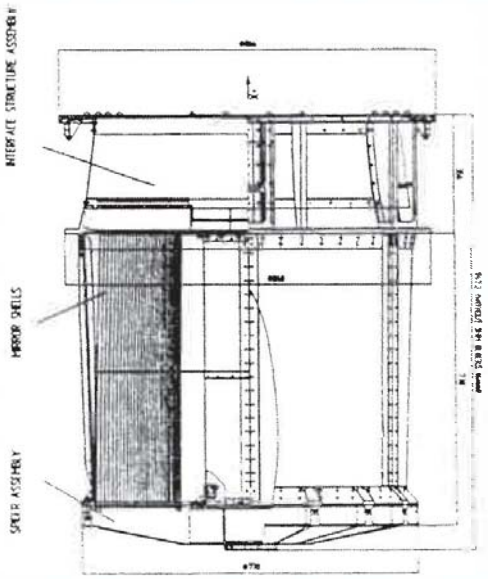

***Figure 4**. Mechanical design of the XMM Mirror Module*

The mechanical design of the Mirror Module is shown in figure 4 and is detailed in reference [8].
When designing the Mirror Module, a constant care was taken for limiting the stray light contribution of any non optical surface viewed by the detectors by:

- limiting the reflectivity of the back side of the mirrors at grazing angles to less than 50%
- roughening of the spider and of the electron deflector walls (roughness > 1 µm rms)
- adding a blocking shell to create the same optical constraints for the innermost mirror as for the others
- having a labyrinth to limit the stray light path between the outermost mirror and the Mirror Interface Structure.

3- OPTICAL STRAY LIGHT ANALYSIS

3.1 Approach

While the geometry of the XMM telescope is both unusual and complex, the approach for performing the stray light analysis was entirely standard. Firstly, a computer model of the telescopes was built with ASAP, a commercially available non sequential ray trace program [12]. Secondly, rays were traced backward from the detector to identify all objects that were visible from the detector. These are called "critical objects", because 100% of the stray light comes from these objects. If an object cannot be seen (either directly, or by reflection or refraction), then it cannot scatter light to the detector. Thirdly, rays were traced forward through the XMM optical system to identify directly illuminated objects. Fourthly, first order (single scatter) stray light paths were identified by objects that are both critical and illuminated, and second order paths were identified by finding ways that light could propagate from the directly illuminated objects to the critical objects. Finally, ASAP was used to make quantitative calculations of the amount of light scattered in the detector. Ray traces were performed in which rays incident on the XMM surfaces were split into scattered rays that propagated to the detector. The accumulated flux on the detector was then used to calculate the detector irradiance, expressed as a Point Source Transmittance, defined as the integrated stray light irradiance at the detector divided by the source irradiance at the entrance to the telescope. In practice, the long and complex ray traces were performed over several months, and required many thousands of CPU hours on Pentium© class computers.

There are three contributors to the total Point Source Transmittance (PST) in the XMM telescope:

- the scatter including all stray light paths in which light is scattered by one or more surfaces
- the diffraction around the edges of the mirrors and of the X-ray baffle
- the throughput, which is the unwanted light that propagates to the detector by specular reflections from the mirrors or sometimes a reflection from the zero order of the gratings.

Figures 5 and 6 show the PST of telescopes 1 and 2 (the ones with the gratings), on the EPIC and RGS detectors, with annotations indicating the one or two main contributors at each point along the curve. For the telescope 3 (the one without the gratings), the PST on the EPIC detector is similar to telescope 2, with the exception of the scatter effect from the gratings. Due to the complex geometry of the telescope, the stray light analysis reveals rather unusual contributors or stray light paths. The next sections present an overview of four stray light problems that are unique to XMM.

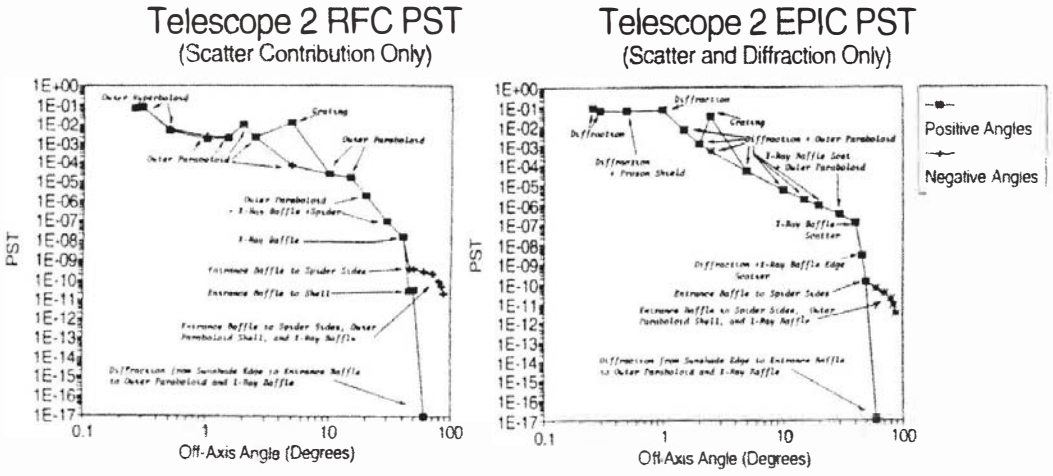

Figures 5 & 6: Point Source Transmittance of the telescope 2 on the RGS (left) and EPIC detector (right)

3.2. Alternative specular paths through the mirrors

The gaps between the mirrors that allow on axis light to reflect and pass between the mirror shells also open up undesired views to the outside. In fact, single reflection paths create a ring of response around the desired Field of View (FOV) that extends for angles between 0.4° and 1.3°. Most of the offending rays may be blocked by inserting auxiliary aperture stops (X-ray Baffle) in front of the mirror shells. The design for these aperture stops takes the form of two sets of concentric rings (sieve plates) inserted at two axial locations in front of the shells (see sections 4 and 6). Figure 7 shows the geometrical collecting area of the telescope 3 as a function of off-axis angle, for three cases: no X-ray Baffle, a perfect X-ray Baffle and an X-ray Baffle with random misalignment, corresponding to known manufacturing errors. The X-ray Baffle does not affect the on-axis collecting area and reduces the off axis light (at angles between 0.5° and 1.2°) by a factor of five.

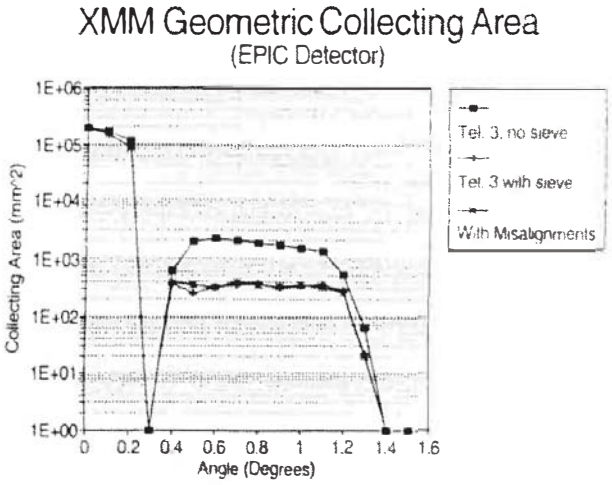

***Figure 7**: X-ray Baffle effect on the geometrical collecting area of the XMM telescope*

3.3 Grazing incidence scatter from the back side surface of the mirrors

In XMM optics, both sides of the paraboloid section of the mirrors are illuminated and are seen by the detectors. The result is a single scatter grazing incidence path to the detector. Calculating the importance of these paths is difficult because the scatter properties of materials are rarely measured at grazing angles. Bidirectional Reflectance Distribution Function (BRDF) measurements were made at grazing incidence on representative mirror samples at ESTEC. A mathematical model was used to fit the measured data within a factor of 2 over almost all incident and scatter directions (even at grazing angles).

The importance of scatter from the back surfaces of the shells is illustrated in figure 8, which shows the contribution of different areas of the mirror to the PST. The figure shows that the backside of the paraboloid of the mirrors contribute much more stray light than the reflective surfaces over off axis angles from 0.5° to 40°.

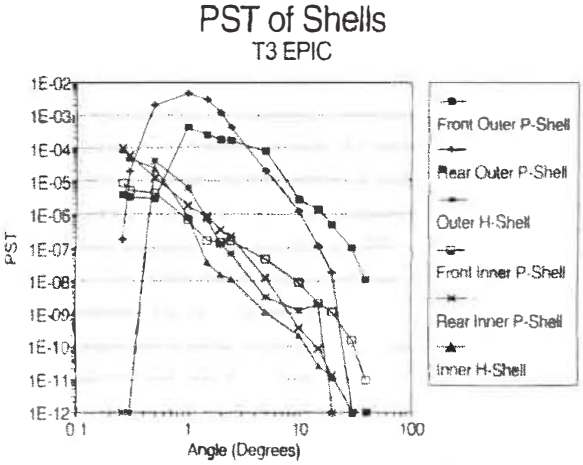

***Figure 8**: Mirror contribution to the Point Source Transmission*

3.4 Grazing incidence reflection and scatter from the gratings

The gratings, that disperse X-rays to the RGS detector, are also responsible for some unusual stray light paths at visible wavelengths. Grazing incidence reflections from the back sides of the gratings

open up views to the outside world, for both the EPIC and the RGS detectors. Fortunately, reflections of this type occur only over a limited range of incoming directions. Stray light paths of this type illustrate the value of stray light analysis even when no corrections to the system are practical. Because the offending area is small, good observations can be made simply by orienting the spacecraft so that bright objects stay outside the area.

3.5 Diffraction from the baffle edges

Edge diffraction occurs whenever an aperture or obstruction imposes a shadow on incoming light. The discontinuity in the irradiance across the shadow boundary causes light to be diffracted out of the incident beam. When some of this diffracted light goes to a detector, it becomes stray light. The edge diffraction calculations were performed using the boundary diffraction wave approach documented in reference [12].
Edge diffraction in the XMM telescope is particularly severe because of the large number of edges. Instead of one or two edges that are present in a conventional system, there are almost 400 edges (due to mirror inner and outer apertures and X-ray baffle vane strip edges - see section 6) that are directly visible by the detectors and therefore can contribute stray light. XMM experiences edge diffraction effects whose magnitude is over 200 times larger than for a conventional telescope system. To illustrate differently the importance of the edge diffraction in XMM telescope, the ratio between the total PST of the XMM telescope and the contribution of diffraction to the PST, as function of the off-axis angle, never exceeds one order of magnitude for angles up to 50°, angle at which the mirror and the X-ray Baffle edges are completely shadowed by the Entrance Baffle and therefore no diffraction occurs anymore.

3.6 Conclusions

For the EPIC detectors behind all the telescopes, stray light from the Earth, the Moon, Jupiter and 0-magnitude stars exceed the specification for the small angles. At the large angles (over 70° for the earth, over 40° for the moon, over 2° for Jupiter and over 1.5° for 0-magnitude stars), the stray light levels drops below the specification. For the Earth, the angle value is worst case assumption: in all the analysis, it is assumed that the Earth subtends a full angle of 18° with an albedo of 0.39, at an altitude of 40000 km (corresponding to the lowest altitude for observations). Therefore, for instance, for an observation with the Earth half illuminated and 80000 km away from XMM, the avoidance angle can be reduced to 47-48°. Also, it is to be noted that in all analysis, the EPIC detector is in open position (no filter) which will correspond only to about 10% of the observation cases.
At 40-46°, the X-ray Baffle is the largest stray light contributor, because it is directly illuminated, while the mirrors are shaded by the Entrance Baffle. At other angles, the X-ray Baffle doesn't significantly increase the stray light at the EPIC detector. This is because scatter from other components also contributes significantly to stray light and this stray light is reduced by partial shading from the X-ray Baffle. Also, the addition of the X-ray Baffle doesn't significantly increase diffraction at small angles (between 2 and 40°). This is due to the fact that the upper sieve shadows some of the edges of the lower sieve and the mirrors.

For the EPIC detectors behind the telescopes 1 and 2 (equipped with the gratings), the gratings do block some stray light by a factor of two, but this is not really an improvement because the on axis X-ray light is also reduced by a factor of two. Scatter from the back side of the gratings increases the PST at +2.5° by a factor of 30 compared to the telescope 3, creating some sharp ghost images on the detector. But this concerns only a solid angle of one degree^2 around and therefore problems can be avoided by keeping bright sources outside of this region.

Concerning the RGS detectors behind the telescopes 1 and 2, stray light levels are equivalent to the ones for the EPIC detector. For the observations, this will impose the same operational constraints

as described in the above. In addition, there is an effect due to the scatter from the back side of the gratings which increases the PST at +5° by a factor of 100 compared to the value at -5°, creating some sharp ghost images on the detector. But this concerns only a three degree ^{2} solid angle and therefore problems can be avoided by keeping bright sources outside of this region.
Stray light from diffraction is absent at small angles over most areas of the RGS, because of the off axis position of the detector, which prevents it viewing large portions of the mirror and X-ray Baffle edges. The X-ray Baffle reduces the throughput to the RGS detector by a factor of 2 for most off-axis angles. Further details on the analysis can be found in reference [9].

4- X-RAY STRAY LIGHT

4.1 X-ray stray light analysis

X-ray scattering will occur for the imaging and dispersion reflections in the mirror system and the grating assembly and this will result in an extended halo around each source observed. This is an intrinsic property of the mirrors and the gratings and can only be suppressed by improving the quality of the mirror and grating surfaces. Every effort has been expended to keep the scattered component to just a few percent of the focused flux.
All the surfaces in the XMM optics will only reflect X-rays at grazing incidence, at angles less than a few degrees. At larger angles, the X-rays are totally absorbed. The level of specular reflection and scattering depends critically on the angle of incidence, the composition (electron density and absorption edges in the atoms) and the surface finish of the gold reflective surface of the mirrors. The gold reflective surfaces have an rms roughness in the order of 3-5 Å, while the back side of the mirror shells and other components in the optics train have a surface finish many orders of magnitude larger.

Extensive Monte Carlo ray tracing of a model of the XMM optical system has been used to evaluate the stray light. All the elements of the telescopes and of the detectors (see sections 1 and 2) were included in the modelling. Fresnel's equations and first order scattering theory combined with the best available optical constants for soft X-rays were used to predict the specular and scattered X-ray levels. The major sources of stray X-rays identified were rogue reflections from mirror or grating surfaces and reflection or scattering from the spider arms, the rear of the mirror shells or the rear of the grating plates. At small off-axis angles up to 1.5 °, the contribution of back surface reflections in the detectors is small and the rogue reflections, none or just one reflection from the mirror gold surfaces, dominate. At larger off-axis angles, the situation is reversed and the diffuse stray flux is dominated by back surface reflections.

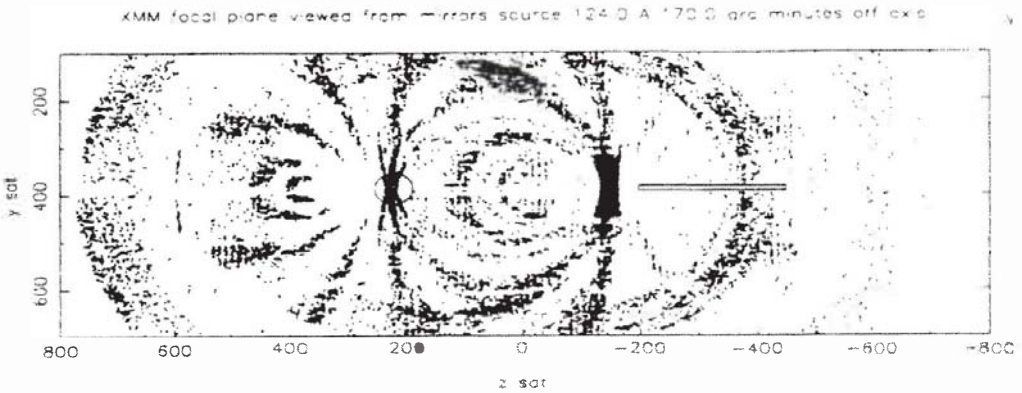

***Figure 9**: Ghost images in the focal plane detectors (EPIC = circle and RGS = rectangle) generated by the rear of the grating plates and the spider arms*

Reflection on the nominally flat surfaces of the spider arms and the backs of the grating plates produces virtual or ghost images of X-ray sources which can end up in the active FOV of the detectors. Although reflection from these surfaces is weak and although the X-ray scattered because of surface roughness, these images can be reasonably well focused in the detector plane and may cause confusion with the true image.
For example, a source at 170 arcmin off-axis in the dispersion plane of the RGS results in a true focused image just next to the short wavelength end of the RGS detector array and is out of focus because of the relatively large off-axis angle. A ghost image reflected from the rear of the grating plates is also seen as a sharp line across the centre of the EPIC field of view (see figure 9).

The effective aperture area at the EPIC and RGS detectors associated with diffuse and ghost X-ray flux was estimated as a function of off-axis position and photon energy using ray tracing runs incorporating several million rays. The largest off-axis angle attempted was 5° and rays were only detected up to an off-axis angle of 4.8°. Beyond this, the stray levels are so low that the calculation of absorption and reflectivities is unreliable (rays are typically suffering more than 10 reflections). From the ray tracing statistics, an upper limit of 0.03 cm^2 on the collecting area for source positions at off-axis angles greater than 5°, can be derived.

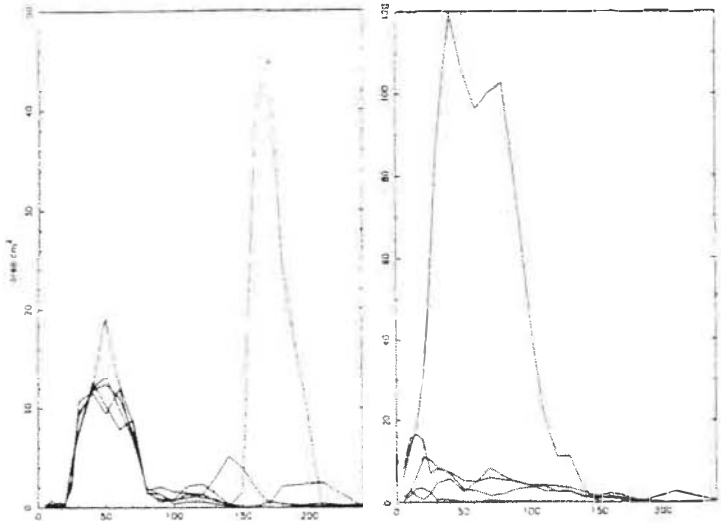

Figures 10 & 11: Off axis collecting area (cm^2) for stray X-ray in EPIC (left) and RGS detector (right) at 0.25 keV (each plot consist of a series of curves taken at different azimuthal angles around the FOV)

Figures 10 and 11 show that the stray X-ray effective area in EPIC due to the ghost images from the spider is in the order of 1 cm^2, at off-axis angles less than 20 arcmin. Increasing to larger off-axis angles there is a major peak of 15 cm^2 at around 50 arcmin due to single reflections from the edge of the hyperboloid section of the mirrors. At one specific azimuthal angle, there is a second peak of 7 cm^2 in the EPIC detector at about 170 arcmin. This is due to the ghost images and only occurs over a small range of azimuthal angles. There is a low level plateau at larger off-axis angles due to back surface reflections.
The stray X-ray aperture areas for the RGS detector lie below 20 cm^2 and fall monotonically with increasing off-axis angle. Over a small range of azimuth zero order reflection gives a rather large broad peak of maximum 100 cm^2. This appears as a halo of scattered X-rays clustered around the true zeroth order image that falls directly onto the RGS detector for source positions in or near the dispersion plane of the gratings.

As indicated in section 2, the ghost images and multiple reflection scattering has been reduced by increasing the roughness of the spider and rear surfaces of the mirror and grating elements. The measured roughness of the rear of the mirrors is Ra 1.3 μm and if all the relevant surfaces have such a finish then the stray light is dominated by zero and single reflections from the mirrors themselves.

4.2 The need for an X-ray baffle

Single reflections from one or more of the hyperboloid surfaces introduce a high level of confusing stray flux in the field of view. This occurs for objects located close to, but outside, the field of view. This must and can only be suppressed using a "precollimator" (or X-ray baffle) consisting of thin cylindrical shells which extend the mirror shells forward. These shells must taper towards the top, to prevent vignetting of the outer edges of the active FOV of the detectors. In order to reduce reflection and scattering from the cylindrical surfaces, cylindrical sections can be removed leaving thin circular annular rings (strips) in front of each mirror (see principle in figure 12).

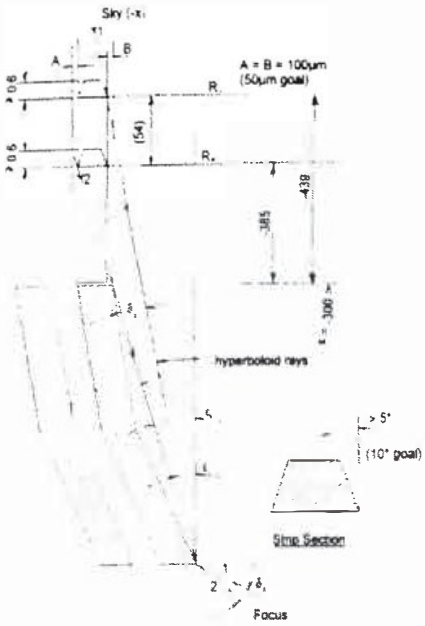

Figure 12: X-ray Baffle opto-mechanical principle

Previous X-ray telescopes with a small number of mirrors could be protected from such effect by such individual shells in front of each mirror. But, highly nested telescopes, such as ASCA, are not baffled due to the limited space between the mirrors. This represents a major limitation for ASCA producing significant stray light and complicating the evaluation of the observation data.
However, for XMM a solution has been found by the XMM team by designing an X-ray Baffle placed in front of the Mirror Module. Thus, the X-ray Baffle is constructed as a series of "sieve plates", made out of circular strips, as described in section 6. These plates are mounted accurately to sit directly in line with the front face of the mirrors such that they block single-reflection- rays but do not eclipse the bona fide two-reflection-rays. The axial space available allows for two such plates to be incorporated into the X-ray Baffle. This blocks about 80% of the rogue, single-reflection-flux.

The total stray X-ray collecting power of the optics is determined by integrating the effective area to stray X-rays over the sky around the field of view for the EPIC or RGS detectors. Assuming a surface roughness of Ra 1.3 µm for the rear surfaces of the mirror shells, the results for 0.1 and 0.25 keV are shown in table 1. The figures drop rapidly with increasing energy above 0.5 keV. With the X-ray Baffle, these figures are reduced by a factor of about 5, which not surprisingly is consistent with the results of the optical stray light analysis in section 3.

	0.1 keV	0.25 keV		0.1 keV	0.25 keV
EPIC	17.9	15.3	RGS	18.7	3.8

Table 2: The low energy collecting power (in $cm^2.deg^2$) without the X-ray baffle

The stray X-ray collecting areas should be compared with the on-axis collecting area of 720 cm^2 below 1 keV for the telescopes equipped with the gratings, the EPIC field of view which is 0.2 $degree^2$ and the RGS field of view which is 0.15 $degree^2$.
The maximum collecting area for ghost images of point sources in EPIC is 7 cm^2 at 0.1 keV, which is 2% of the on-axis collecting area for the telescopes equipped with the gratings or 1% for the telescopes without the gratings. Therefore, sources which are about 100 times as bright as the target just outside the field of view can produce count rates in ghost images which are of the same order as the target rate.

The soft X-ray spectrum of the sky background from ROSAT observations is reasonably well represented by the sum of a low temperature thermal component T=1.5 10^6 K and emission measure 1.0 10^{-3} cm^{-6}.pc. sec^{-2} str^{-1} and a power law, photon index gamma 1.7 and normalisation 11 keV cm^{-2} pc. sec^{-1} str^{-1} keV^{-1}. This spectrum can be folded through the energy response of the optics, including the blocking of the X-ray baffle and assuming a rear surface roughness of Ra 1.3 µm. Thus, the stray X-ray count rate to be expected from the diffuse background, can be estimated. The results are given in table 2. The rates are highest in the C-band which is 0.1 to 0.28 keV, but they are all less than 5%, which is reasonable.
Further details on the analysis can be found in references [13, 14, 15].

	True image (photon.sec^{-1})	Stray X-rays (photon.sec^{-1})	Ratio Stray X-ray by True image (%)
EPIC total	1.734	0.056	3.2
EPIC C-band	0.654	0.032	4.8
RGS total	1.345	0.03	2.2
RGS C-band	0.507	0.018	3.5

Table 2 Stray X-ray photon rates sec^{-1} from the diffuse background compared with the rates for the true image of the same background (X-ray baffle blocking included, but detector efficiency and filter transmission not taken into account)

5- ENTRANCE BAFFLE DESCRIPTION

The three Entrance Baffles are identical cylindrical aluminium structures with an outer diameter of 870 mm. Their inside is covered by 12 circumferential vanes and is optically black. Due to volume constraints under the Ariane 5 launcher fairing, the baffle length is limited to 900 mm, including the protrusion of 200 mm below the separation plane into the launch adaptor.

Apart from its primary function of reducing stray light, the Entrance Baffle has to fulfill the following requirements:

- to stay aligned with the Mirror Module (± 0.5 mm) to avoid obscuration and stray light from the circumferential vanes
- to be thermally decoupled from the Mirror Support Platform (max. conductive heat flux < 5 W) in order to have a stable thermal environment for the telescope
- to provide a gas and light tight interface with the Mirror Module
- to allow radial and lateral relative displacements of the spider of the Mirror Module without generating significant loads
- to have a resonance frequency higher than 95 Hz.

These requirements have to be satisfied in severe environmental conditions which envelope the service life on XMM spacecraft:

- axial thermal gradient along the Entrance Baffle from -105 °C up to -40 °C
- acceleration of 50 g in any direction.

In order to limit the mechanical loads on the Mirror Module, the solution is to mount the Entrance Baffle isostatically on the Mirror Support Platform, by the means of three stiffening webs, which are stiff in the tangential direction and much less stiff in the radial direction. In this way, the Entrance Baffle cylinder is allowed to "expand", while firmly fixed on the Mirror Support Platform. Several analyses were performed to define and optimise the blade configuration (width, position, taper,

thickness and material) in order to fulfill the stray light requirement and the mechanical requirements, while keeping the Mirror Support Platform induced distortions within acceptable limits.

After some design considerations, the taper on the location of the vane edges was chosen to be 2°. This small taper angle allows relatively deep vane cavities and therefore a few vanes are sufficient to eliminate small first order scatter paths from the Entrance Baffle to the telescope aperture. Also, attention was paid on the orientation and the angles of the bevels (vanes), which depends on their axial position, in order to reduce direct scatter paths to the X-ray baffle.
The thermal decoupling was achieved by using a Glass Fibre Re-In forced Plastic (GFRP) material for the fixation blades, limiting the heat flux to less than one Watt. The light and gas tightness requirements were achieved by mounting a bellow, consisting of a sealing made of two MLI Kapton foils (laminated with Kevlar fibres for added strength), between the Entrance Baffle and the Mirror Module. The loads, generated on the Mirror Module, are small and the heat conduction is negligible (below 0.1W).

6- X-RAY BAFFLE (XRB) DESIGN AND MANUFACTURING

6.1 X-ray baffle design

The X-ray Baffle is one of the major technological challenges of the XMM spacecraft development to be completed in a short time. From the decision to reduce the X-ray stray light by the implementation of an X-ray baffle, it took only seven months to the XMM Project to:

- design the X-ray baffle
- demonstrate the feasibility of manufacturing the sieve plates within required tolerances
- verify that the performance of the telescope was not degraded in terms of resolution, effective area and optical stray light
- redefine the mechanical interfaces
- redesign the entrance baffle,

all this, at a very late stage in the XMM program (after the start of the C/D phase).

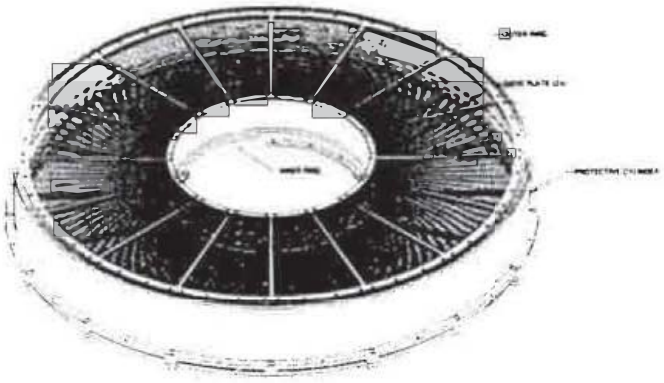

Figure 13: 3D view of the X-ray Baffle

The X-ray Baffle has a cylindrical shape (see figure 13) with an outer diameter of 770 mm and a height of 108 mm. Its total mass is about 10 kg. The heart of the X-ray Baffle are the two sieve plates axially spaced by 54 mm, which perform the "blocking" function (see figure 12). The other parts provide support (inner ring and outer ring) and mechanical protection (protective cylinder) to the fragile sieve plates.
Each sieve plate is basically a disc with 59 circumferential strips and 16 radial spokes, therefore with 58 x 16 slots. The outer diameter of the disc is 728 mm and its thickness is 1 mm, except for the stiffeners located on the spokes and the outer annular ring, where the thickness is 5 mm. In order to reduce to a maximum extent, the optical stray light, that is introduced by the X-ray Baffle, the lateral surfaces of the strips are chamfered by 5° and the edges of the strips are made very sharp (radius < 20 μm). All the surfaces of the X-ray Baffle (including the edges of the vane strips) facing the mirrors are blackened.

The main requirement placed on the X-ray Baffle is the accuracy of the radial position of the circular edges of the vane strips of the sieves with respect to the position of the mirrors. It must be better than 100 µm, including manufacturing, assembly and integration errors and displacement due to thermal conditions (-10°C/ +10°C).

The fulfilment of the "blocking" function within this tolerance (100 µm) relies on:

- the minimisation of the displacements of the X-ray Baffle due to thermal conditions, by selecting a high quality Invar material, with a very low coefficient of thermal expansion (lower than $10^{-6}.°C^{-1}$), for the sieve plates and their support structure (inner and outer ring)
- the accurate machining of each sieve plate.
- the accurate assembly of both sieve plates on their support structure (relative positioning)
- the accurate positioning of the X-ray Baffle on top of the Mirror Module.

Each of these aspects has been carefully analysed and implemented, as it is explained here below.

6.2 X-ray Baffle sieve plate manufacturing

The machining tolerance defined for the radial position of the circumferential edges of the strips of the sieve plates is 65 µm, which is a tight tolerance taking into account that the sieve plates are large and flexible. This tolerance has been the driver to define the manufacturing process to machine the slots. After having analysed several potential machining processes (among them photochemical etching and laser cutting), the Wire Electrical Discharge (WED) machining has proven to be the most adequate, although it has the disadvantage of requiring long machining times. Each sieve plate needs between 400 and 500 machining hours, which led to the use of two WED machines in parallel for the production of 4 X-ray baffles (i.e. 8 sieves) in due time.

Each sieve plate (see figure 14) is produced in two phases: the pre-machining and the WED machining. The pre-machining starts from a thick flat disc, which is machined to its final shape except for the slots. A flat 1 mm thick disc with 5 mm thick stiffeners and all the attachment holes is obtained. Then, after having drilled one start hole per slot (928 slots per sieve plate), the slots are cut by electro-erosion on the WED machine. Several WED machining tests were performed before starting the manufacturing of the sieve plates, in order to define an adequate process (machining sequence, number of cuttings, cutting speed,...).

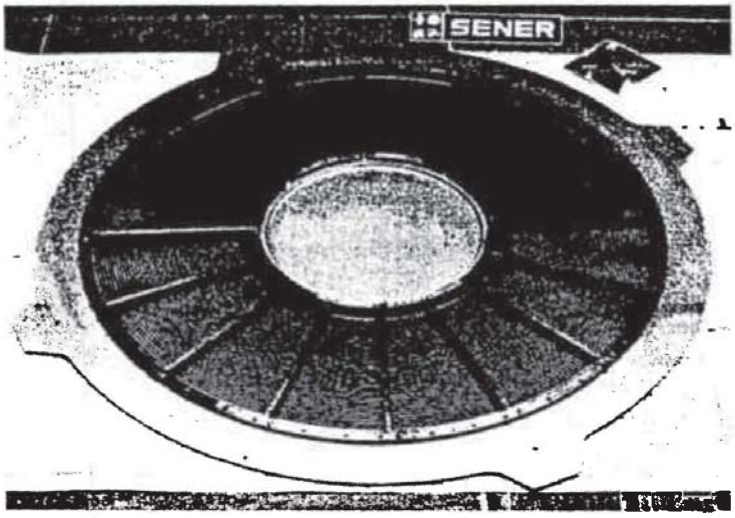

Figure 14: X-ray Baffle sieve plate

The verification of each sieve plate is performed on a 3D measuring machine. The radial position of the edges respect to the center of the sieve plate is measured at 10 points per slot, I. e. 9280 points per sieve plate. The results obtained with the chosen WED machining procedure are very good, with mean value of the radial errors of about 25 µm with a standard deviation of about 35 µm.

6.3 X-Ray Baffle assembly and installation on the Mirror Module

First of all, both sieve plates are assembled using as reference some accurate holes machined in the sieve plates and on the inner ring, leading to a good initial relative positioning. Then, the relative positioning between both sieve plates is measured with a 3D measuring machine. If the misalignment between both sieves is higher than the defined limit, the relative positioning is corrected by means of a special adjustment device designed for this purpose.

The accurate positioning of the X-ray Baffle on the Mirror Module is achieved by taking, as reference, the location of the center of the mirror nesting with respect to two reference points on the Mirror Module spider and the location of the center of the X-ray Baffle with respect to two reference points on the X-ray Baffle structure and then performing the corresponding alignment of those centers.

Once the integration has been performed, an optical test (effective area measurement at various off-axis angles in two orthogonal directions) allows to check if the performance of the telescope remains unchanged after the mounting of the X-ray Baffle (no vignetting effect). This is to confirm that the correct positioning. If not, another optical test (X-ray pencil beam) is performed to evaluate the misalignment between the mirrors and the X-ray Baffle, so that the X-ray Baffle may be moved with respect to the Mirror Module to correct for to the measured misalignment.

7- STRAY LIGHT TEST AND VERIFICATION

Stray light tests are planned in the visible and near-infrared spectral range, in order to verify the predictions obtained from the stray light calculations. These tests are foreseen at

small angles, up to 7.5°, with the complete telescope, with the exception of the Entrance Baffle

large angles, from 5° up to at least 47°, with the complete telescope.

Other spacecraft components (i.e. Telescope Sun Shield and Telescope Tube) are not present in this test due to their large dimensions. They are not considered as important verification subjects, because the analysis has shown that the corresponding stray paths lead to negligible stray light contributions.

The test configuration will include the telescope with and without the gratings. The test detector will be placed at the position of the EPIC camera and of the RGS detector.

7.1 Small angle test

For small angles of incidence, the test facility of the Centre Spatial de Liège (Focal X) will be used. Focal X is providing a vertical full aperture collimated beam in Extreme Ultra Violet and in visible light under vacuum. To achieve off axis measurements up to 7.5°, the lower optical bench (supporting the tested telescope), the tower and the upper optical focal bench (made out of one single piece of structure) can be tilted. Detailed description of the facility, developed by the XMM Project for the characterisation of the optical performance of the XMM telescopes, is given in reference [6].

End 1996, some preliminary tests performed with the Qualification Model of the Mirror Module alone have already demonstrated that the facility presents no measurable stray light and that the correlation between the model and the measurement was very good.

7.2 Large angle tests

Large angle tests will be performed in the clean room (class 100) of Dornier (Munich - Germany). The test-setup is sketched in figure 15, in the case of telescope no. 3, i.e. the one without gratings. It includes the light source with a Xenon-arc lamp, the collimator and the tested telescope. The test detector is at the position of the EPIC camera, where the Point Source Transmittance (PST) is measured and compared with the analysis results.

The estimation of the signal to noise ratio (S/N) shows that the chain with the source, the optics, the XMM telescope and the chosen CCD test detector is not noise limited. In fact, it is limited by the scattering of the air and dust and by the backscattering from the walls of the test facilities within the direct field of view of the telescope.

The large dimensions of the test set-up led to the decision not to perform the stray light test in vacuum. Therefore, scattering of the air and dust will cause a background PST of the order of 10^{-4}, in spite of the high cleanliness of the test facility and of the exclusion of the blue and green part of the spectrum of the Xenon lamp. The backscattering is coming from the telescope elements towards the direction of the direct field of view (a light trap is placed there) and from the light trap itself. Although the backscattering by the light trap is minimized by applying material with the lowest possible Bidirectional Reflectance Distribution Function (BRDF), there will be a residual background PST of the order of 10^{-4} from the light trap, due to its large size.

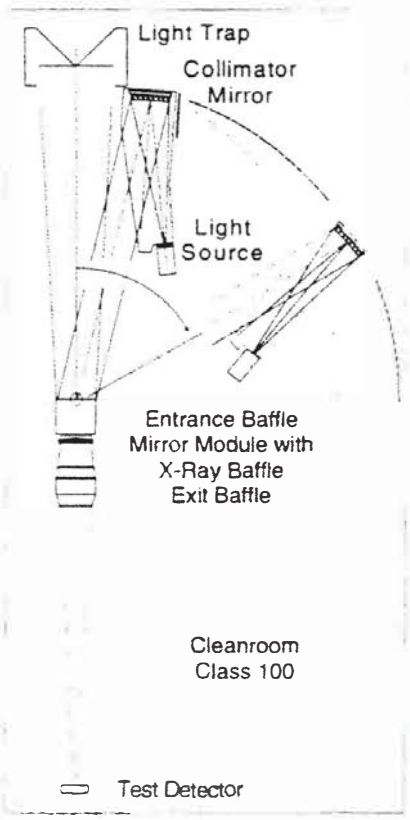

***Figure 15**: Large angle test set-up for stray light measurements*

In conclusion, the stray light calculations can be verified for a large range of angles of incidence of the incoming radiation. Thus the optical mathematical model can be validated to a large extent. Only the small values of PST occurring at angles approaching 90° cannot be verified, due to air and dust scattering and due to backscattering from the light trap in the direct field of view.

8- CONCLUSIONS

A remarkable and unprecedented work in X-ray telescope has been performed and conducted by the XMM team. This work includes :

- the detailed analysis of the optical and the X-ray stray light
- the design and the manufacturing of the X-ray baffle with high precision machining.

This effort on the X-ray baffle was decided as it was clear that the scientific value of the XMM mission could be improved by reducing the out of field of view X-ray sources. The X-ray baffle will be efficient for the blocking of undesired light (about 80%) in the X-ray domain. Its position in front of the telescope presented the risk of a significant increase of optical stray light, due to its large number of edges. The X-ray baffle has been proven not to increase the optical stray light level, except for angles between 40 and 46°, where the Point Source Transmittance levels go up by a factor of 10.

Operations will ensure that the Earth limb does not come in this area.

The manufacturing of the sieve plates of the X-ray Baffle is a technological challenge. The position accuracy needed on the fragile and flexible sieve plates required machining by electro erosion on highly accurate machining stations. Three complete X-ray Baffles have been produced and are delivered. Optical and environmental tests are now proceeding at Centre Spatial de Liège in order to qualify its design.

Quoted from the conclusions of the report of the Review of the XMM Telescope System, held in September 96 at Estec:

> *"A remarkable and unprecedented work on stray light analysis has been performed and conducted by the XMM Project.*
> *A remarkable on image quality has been performed by the Project, which will facilitate scientific interpretation".*

9- ACKNOWLEDGEMENT

The work on the optical and X-ray stray light has been conducted in the frame of the ESA XMM contract 11860/96/NL/RE by ESA and Dornier (Friedrichshafen, Germany) with the support of .

Breault Research Organization (BRO), Inc (Tucson - Arizona - USA) for the optical stray light analysis
Centre Spatial de Liège (Liège - Belgium) for the testing of the XMM telescopes
Dornier (Ottobrün - Germany) for the design and the development of the test set-up for the stray light test at large angles
Oerlikon Contraves (Zurich - Switzerland) for the design and the manufacturing of the Entrance Baffles
Österreichische Raumfahrt und Systemtechnik (ORS) Gmbh (Vienna - Austria) for the design and the manufacturing of the Exit Baffles
Sener (Las Arenas - Spain) for the manufacturing of the X-ray Baffles.

The authors wish to especially acknowledge Martine Joubert of Centre National d'Etudes Spatiales (CNES) for her assistance in the review of the XMM telescope.

Members of the Telescope Advisory Group, Dr. B. Aschenbach from the Max Planck Institute of Garching, Dr. P. de Korte from Space Research Organisation Netherlands of Utrecht and Dr. R. Willingale from University of Leicester, as well as ESA personnel are thanked for their continuous support during this development.

Our congratulations go also to R.P. Breault of BRO, for his precious advice. Thanks are also due to T. Weigel of Retocon (Eggersriet - Switzerland) for making measurements of BRDF and for fruitful discussions.

10- REFERENCES

1. J. van Casteren - "XMM, a large telescope" - SPIE Proc. 2808, pp. 338-349, (1996)

2. P. Gondoin, D. de Chambure, K. van Katwijk, P. Kletzkine, D. Stramaccioni, B. Aschenbach, O. Citterio, R. Willingale - "The XMM Telescope" - SPIE Proc. 2279, pp. 86-100, (1994)

3. D.H. Lumb, H. Eggel, R. Lainé, A.J. Peacock - "X-ray Multi mirror Mission: an overview" - SPIE Proc. 2808, pp. 326-337, (1996)

4. J.P. Collette, C. Jamar - "X-ray and Extreme Ultra Violet Facility for the XMM Optics" - IAF - Oslo 1995

5. R. Lainé, D. de Chambure - "XMM X-ray mirror technological development" - AAAF Symposium on Scientific Satellite Achievements and Prospects in Europe - Paris 1996

6. R. Lainé, D. de Chambure - "Results of the Thin X-ray Mirror Technology for the ESA XMM Mission" - IAF - Torino 1997

7. D. de Chambure, R. Lainé, J. van Casteren, K. van Katwijk, P. Glaude - "Producing the X-ray Mirrors for ESA's XMM Spacecraft" - ESA Bulletin 89, pp. 68-79, (1997)

8. D. de Chambure, R. Lainé, J. van Casteren, K. van Katwijk, P. Glaude - "The Status of the Flight X-ray Mirror Production for the XMM Spacecraft" - SPIE Proc, (1997)

9. G.L. Peterson, M. Côté - Lessons Learned from the Stray Light Analysis of the XMM Telescope" - SPIE Proc, (1997)

10. D. Willingale - "The XMM Electron Diverter" - University of Leicester - February 1995

11. Max Born and Emil Wolfe - Principles of Optics, Sixth ed. (Pergamon Press, New York, 1980), pp 449-453

12. Advanced Systems Analysis Program (ASAP), a product of Breault Research Organization Inc., Tucson, Arizona

13. D. Willingale - "Stray X-ray Scattering in XMM" - University of Leicester - November 1995

14. B. Aschenbach - "The Impact of X-ray Stray Light on the Scientific Performance of XMM" - XMM-TS-FMP005 - Max-Planck-Institut für Extraterrische Physik - January 1996

15. P. Gondoin - X-ray Analysis of a XMM Mirror Module equipped with X-ray Baffles" - XMM-PS-TN06, Iss.1 - ESTEC - May 1996